Computers and Fluids 172 (2018) 196–208

Contents lists available at ScienceDirect

Computers and Fluids

journal homepage: www.elsevier.com/locate/compfluid

Benchmark solutions

A perturbational weighted essentially non-oscillatory scheme

Fangjun Zeng[a,b], Yiqing Shen[a,b,*], Shengping Liu[a,b]

[a] State Key Laboratory of High Temperature Gas Dynamics, Institute of Mechanics, Chinese Academy of Sciences, Beijing 100190, China
[b] School of Engineering Science, University of Chinese Academy of Sciences, Beijing 100049, China

ARTICLE INFO

Article history:
Received 7 December 2017
Revised 11 May 2018
Accepted 6 July 2018
Available online 9 July 2018

Keywords:
WENO scheme
Numerical perturbation method
Necessary and sufficient conditions
Low-dissipation

ABSTRACT

In this paper, based on the perturbed fluxes of all candidate fluxes used in the traditional fifth-order WENO scheme, a fifth-order accurate perturbational weighted essentially non-oscillatory (P-WENO) scheme is developed. First, a corollary about the accuracy of a kind of conservative schemes is generalized and proved. Then, based on the corollary and the idea of numerical perturbation, the perturbed fluxes, which are one order higher than the traditional candidate ones of the fifth-order WENO scheme, are obtained. Furthermore, we derive the necessary and sufficient conditions for the fifth-order convergence of the new weighted scheme constructed by using the new perturbed fluxes and find that they are one order lower than those derived by Henrick et al. for the traditional fifth-order WENO scheme. Thus, the new weighted scheme, which uses the same weights of the WENO-Z scheme and the perturbed fluxes, can meet the necessary and sufficient condition for fifth-order convergence even at critical points. The resulted P-WENO scheme actually provides a novel method to decrease the numerical dissipation of traditional WENO schemes. Numerical examples are presented to verify the accuracy, robustness and low-dissipation of the new scheme.

1. Introduction

The weighted essentially non-oscillatory (WENO) schemes have been widely used in solving compressible flows due to their uniformly high order accuracy in smooth regions and essentially non-oscillatory (ENO) property near discontinuities. The first WENO scheme was proposed by Liu et al. [1]. Subsequently, Jiang and Shu [2] proposed a classical smoothness indicator and a general framework of WENO schemes. Henrick et al.[3] provided a detailed analysis about the accuracy of the fifth-order WENO scheme of Jiang and Shu (WENO-JS) and found that it fails to achieve the optimal order at critical points where the first derivative of the solution vanishes. Meanwhile, they derived the necessary and sufficient conditions on the weights for fifth-order convergence and developed a new fifth-order WENO scheme (WENO-M) which utilizes a mapping function to revise the weights of WENO-JS scheme to satisfy the sufficient condition (SC). After that, the SC was used as a guidance to design the weights for improving WENO schemes.

In [4], Borgers et al. proposed a high order global smoothness indicator to calculate the weights (the WENO-Z scheme). Although the WENO-Z scheme has low dissipation, its weights do not satisfy the SC at critical points of smooth solution and its convergence order is degraded to only fourth-order. Following the idea of the WENO-Z scheme, Ha et al. [5] proposed a new sixth-order global smoothness indicator. Although the authors proved that the resulted WENO scheme can meet the SC at critical points of smooth solution, its numerical results rely on a user-tunable parameter [6]. Fan et al. [7] developed several higher order global smoothness indicators (even up to eighth-order). It is clear that these indicators can recover fifth-order even at critical points of smooth solution. However, numerical results showed that these higher order global smoothness indicators are prone to generating oscillations for solving problems with shock waves [8]. On the other hand, several scholars [9–11] suggested that the parameter ε used to calculate the weights of WENO schemes can be defined as a function of the mesh size Δx to obtain the formal order at critical points. However, it is easy to recognize that the solutions of those resulted WENO schemes lose the scale invariance property, particularly, if the reference length takes a small value, then Δx will be a large value, and hence this kind of scheme may generate numerical oscillations. In order to achieve fifth-order accuracy at critical points and keep low dissipation and ENO property near discontinuities, this paper considers another different way, i.e., how to construct a weighted scheme to relax the restraints of fifth-order convergence.

The numerical perturbation method (NPM) was first proposed by Gao [12] for solving convection-diffusion equation. The main idea of the NPM is that, by multiplying a perturbational polynomial

* Corresponding author.
E-mail address: yqshen@imech.ac.cn (Y. Shen).

https://doi.org/10.1016/j.compfluid.2018.07.003
0045-7930/

(a power-series of grid intervals), then eliminating the truncated error terms in the modified differential equation to get the corresponding coefficients of the perturbational polynomial, and finally the numerical perturbation method is obtained. The advantage of the NPM is that it improves the accuracy of schemes without increasing the total number of grid points. Based on the first-order upwind scheme, Shen et al. [13] developed a second-order perturbational finite difference scheme for hyperbolic conservation equation. Gao et al. [14] extended the idea of the NPM to the finite volume method. Li et al. [15] developed a third-order scheme with modified coefficients based on second-order ENO scheme. Recently, Yu et al. [16] proposed a symplectic and phase error reducing perturbation finite-difference advection scheme.

In this paper, based on the works [17,18], a corollary about the accuracy of a conservative scheme is generalized and proved. And then, combining the NPM and the corollary, we use the perturbed forms of the candidate fluxes used in the WENO scheme to construct a new weighted scheme. We also prove that the new scheme relaxes the sufficient condition for fifth-order convergence of a fifth-order WENO scheme, since the perturbed fluxes are one order higher than their counterparts. Thus, using the weights of the WENO-Z scheme and the perturbed fluxes, the resulted perturbational WENO (P-WENO) scheme can achieve fifth-order accuracy in smooth regions even at critical points.

The rest of this paper is organized as follows: in Section 2, the accuracy of a conservative scheme is discussed and a corollary is proposed. In Section 3, a perturbational WENO scheme is constructed by using the perturbed candidate fluxes. In Section 4, several numerical examples are presented to verify the robustness and low dissipation properties of the proposed scheme. Some conclusions of this paper are given in Section 5.

2. The accuracy of conservative scheme

The one-dimensional hyperbolic conservation laws is used as a model equation to describe the numerical method in this paper,

$$\frac{\partial u}{\partial t}+\frac{\partial f(u)}{\partial x}=0,\qquad t\in[0,\infty], x\in[a,b], \tag{1}$$

where $u(x,t)$ is the conservative variable, $f(u)$ is the flux function.

With an uniform grid spacing Δx, the semi-discretization form of Eq. (1) can be written as

$$\frac{du_i}{dt}+\frac{\hat{f}_{i+\frac{1}{2}}-\hat{f}_{i-\frac{1}{2}}}{\Delta x}=0, \tag{2}$$

where u_i is the numerical approximation of u at node x_i, $\hat{f}_{i+1/2}$ and $\hat{f}_{i-1/2}$ are the numerical fluxes of f at cell interfaces $x_{i+1/2}$ and $x_{i-1/2}$, respectively.

To calculate the numerical fluxes $\hat{f}_{i\pm1/2}$, a function h is implicitly defined as follows [19]

$$f(x)=\frac{1}{\Delta x}\int_{x-\frac{\Delta x}{2}}^{x+\frac{\Delta x}{2}}h(\xi)d\xi. \tag{3}$$

Differentiating Eq. (3) with respect to x, we have

$$\left.\frac{\partial f}{\partial x}\right|_{x=x_i}=\frac{h_{i+\frac{1}{2}}-h_{i-\frac{1}{2}}}{\Delta x}. \tag{4}$$

From Eqs. (2) and (4), we can see that the numerical fluxes $\hat{f}_{i\pm1/2}$ are the approximations of $h_{i\pm1/2}$.

In [17], Shu and Osher concluded that the existence of constants $a_2, a_4, \cdots, a_{2m-2}, \cdots$, such that if

$$\hat{f}_{i+\frac{1}{2}}=f_{i+\frac{1}{2}}+\sum_{l=1}^{m-1}a_{2l}\Delta x^{2l}\left.\frac{\partial^{2l}f}{\partial x^{2l}}\right|_{i+\frac{1}{2}}+O(\Delta x^{2m+1}), \tag{5}$$

then the scheme would be $(2m)$th order accuracy in space, for example, $a_2=-\frac{1}{24}, a_4=\frac{7}{5760},\cdots$.

In [18], Shui gave the relations of the coefficients a_{2l} in Eq. (5),

$$\sum_{l=0}^{k}\frac{a_{2l}}{2^{2k-2l}(2k-2l+1)!}=0,\qquad a_0=1,\quad k=1,2,\cdots,m-1, \tag{6}$$

and then proved the scheme is $(2m)$th order accurate in space.

The two works mentioned above only given the summarization for even-order accuracy of the conservative scheme. Here, we further generalize them to form a corollary, which can also be applied to construct our new scheme.

Corollary. *For the numerical flux*

$$\hat{f}_{i+\frac{1}{2}}=f_{i+\frac{1}{2}}+\sum_{l=1}^{m}a_{2l}\Delta x^{2l}\left.\frac{\partial^{2l}f}{\partial x^{2l}}\right|_{i+\frac{1}{2}}+\tilde{A}\left.\frac{\partial^{2m+1}f}{\partial x^{2m+1}}\right|_{i+\frac{1}{2}}\Delta x^{2m+1}+O(\Delta x^{2m+2}), \tag{7}$$

the coefficients a_{2l} satisfy

$$\sum_{l=0}^{k}\frac{a_{2l}}{2^{2k-2l}(2k-2l+1)!}=0,\qquad a_0=1,\quad k=1,2,\cdots,m, \tag{8}$$

- *if $\tilde{A}\neq0$, then the scheme is $(2m+1)$th order accuracy in space;*
- *if $\tilde{A}=0$, then the scheme is at least $(2m+2)$th order accuracy in space.*

The proof of the corollary is given in Appendix.

3. Fifth-order WENO schemes

3.1. The traditional fifth-order WENO schemes

The numerical flux $\hat{f}_{i+1/2}$ of a fifth-order WENO scheme can be written as

$$\hat{f}_{i+\frac{1}{2}}=\sum_{k=0}^{2}\omega_k\hat{f}^k_{i+\frac{1}{2}}, \tag{9}$$

where $\hat{f}^k_{i+1/2}$ is the numerical flux on the sub-stencil $S_k=(x_{i+k-2},x_{i+k-1},x_{i+k})$,

$$\begin{aligned}\hat{f}^0_{i+\frac{1}{2}}&=\frac{1}{3}f_{i-2}-\frac{7}{6}f_{i-1}+\frac{11}{6}f_i,\\ \hat{f}^1_{i+\frac{1}{2}}&=-\frac{1}{6}f_{i-1}+\frac{5}{6}f_i+\frac{1}{3}f_{i+1},\\ \hat{f}^2_{i+\frac{1}{2}}&=\frac{1}{3}f_i+\frac{5}{6}f_{i+1}-\frac{1}{6}f_{i+2}.\end{aligned} \tag{10}$$

ω_k is the nonlinear weight. In [2], ω_k is calculated as

$$\omega_k=\frac{\alpha_k}{\alpha_0+\alpha_1+\alpha_2},\quad \alpha_k=\frac{c_k}{(IS_k+\varepsilon)^2},\quad k=0,1,2, \tag{11}$$

where $c_0=\frac{1}{10}, c_1=\frac{6}{10}, c_2=\frac{3}{10}$ are the ideal weights; ε is a small positive number introduced to avoid the denominator becoming zero. A detailed discussion of the magnitude and the role of ε can be found in Refs.[2,3]. As suggested in [3], $\varepsilon=10^{-40}$ is used in this paper. IS_k is the smoothness indicator on the sub-stencil S_k. A classical formula for IS_k is proposed by Jiang and Shu [2] as

$$IS_k=\sum_{l=1}^{r-1}\int_{x_{i-\frac{1}{2}}}^{x_{i+\frac{1}{2}}}\Delta x^{2l-1}\left(\frac{d^l\hat{f}^k(x)}{dx^l}\right)^2dx. \tag{12}$$

The explicit form of IS_k for the fifth-order WENO scheme $(r=3)$ can be expressed as

$$IS_0 = \frac{13}{12}(f_{i-2} - 2f_{i-1} + f_i)^2 + \frac{1}{4}(f_{i-2} - 4f_{i-1} + 3f_i)^2,$$
$$IS_1 = \frac{13}{12}(f_{i-1} - 2f_i + f_{i+1})^2 + \frac{1}{4}(f_{i+1} - f_{i-1})^2,$$
$$IS_2 = \frac{13}{12}(f_i - 2f_{i+1} + f_{i+2})^2 + \frac{1}{4}(3f_i - 4f_{i+1} + f_{i+2})^2. \quad (13)$$

Henrick et al. [3] derived the necessary and sufficient conditions for fifth-order convergence of a fifth-order WENO scheme as

$$\sum_{k=0}^{2} A_k'(\omega_k^+ - \omega_k^-) = O(\Delta x^3), \quad (14a)$$

$$\omega_k^\pm - c_k = O(\Delta x^2). \quad (14b)$$

where $A_k' = A_k f_i'''$, and A_k is the same as given in Eq. (18); the superscripts $\pm$ correspond to the numerical fluxes $\hat{f}_{i\pm1/2}$, respectively. And a simple sufficient condition

$$\omega_k^\pm - c_k = O(\Delta x^3), \quad (15)$$

is usually used to guide the construction of a WENO scheme.

Henrick et al. [3] also pointed out that the weights calculated by Jiang and Shu's method Eq. (11) fail to obtain the maximum order at critical points, and they proposed a mapping function to recover the optimal order of convergence.

Borges et al. [4] proposed a different method to calculate the weights by incorporating the higher order information about the regularity of the numerical solution and they gave the formula of the weights as follows

$$\omega_k = \frac{\alpha_k}{\alpha_0 + \alpha_1 + \alpha_2}, \quad \alpha_k = c_k\left(1 + \left(\frac{\tau_5}{IS_k + \varepsilon}\right)^q\right), \quad k = 0, 1, 2, \quad (16)$$

where, $\tau_5 = |IS_0 - IS_2|$ can be called as a global smoothness indicator.

The convergence order of the fifth-order WENO (WENO-Z) scheme [4] at critical points is influenced by the power parameter q in the definition of weights Eq. (16), for example, the accuracy is fourth- and fifth-order if the power q takes the value of 1 and 2, respectively. On the other hand, Borges et al. pointed out that, for solutions containing the discontinuities, increasing q makes the scheme more dissipative, hence $q = 1$ is suggested in [4] and used in this paper, unless otherwise indicated.

Later, in order to improve the accuracy of the WENO-Z scheme and maintain low dissipation (means $q = 1$), several higher-order global smoothness indicators are proposed, for example, two sixth-order formulas [5,7] and two eighth-order formulas [7]. Although those global smoothness indicators can make the weights with $q = 1$ meet the sufficient condition Eq. (15) in smooth regions even at critical points, a user-tunable parameter in [5] and the oscillatory solutions near discontinuities generated in [7] limit the application of those resulted WENO schemes. Therefore, the issue of how to improve the accuracy of the WENO-Z scheme and maintain low dissipation and ENO property is still open.

3.2. The new perturbational WENO scheme

In this section, we introduce the numerical perturbation method to construct a kind of new WENO scheme. The new scheme can reduce the constraint of the sufficient condition from third order to second order, i.e.

$$\omega_k^\pm = c_k + O(\Delta x^2). \quad (17)$$

3.2.1. The construction of the perturbed fluxes

Taylor expansions of Eq. (10) at $x_{i+1/2}$ give

$$\hat{f}_{i+\frac{1}{2}}^k = f_{i+\frac{1}{2}} - \frac{1}{24}\frac{\partial^2 f}{\partial x^2}\Big|_{i+\frac{1}{2}}\Delta x^2 + A_k\frac{\partial^3 f}{\partial x^3}\Big|_{i+\frac{1}{2}}\Delta x^3 + O(\Delta x^4), \quad (18)$$

where $A_0 = -\frac{1}{4}, A_1 = \frac{1}{12}, A_2 = -\frac{1}{12}$.

According to the corollary, Eq. (18) reveals that the numerical fluxes $\hat{f}_{i+1/2}^k$ are third-order accurate. It is natural to think of that, if all these candidate fluxes are improved to fourth order, whether the requirements of the weights Eq. (14) can be relaxed or not. Following this idea, we use a perturbational polynomial P_k of the grid spacing as

$$P_k = 1 + b_k\Delta x^3 + O(\Delta x^4), \quad (19)$$

to multiply the candidate fluxes $\hat{f}_{i+1/2}^k$, and then get the new fluxes $\tilde{f}_{i+1/2}^k$ as

$$\tilde{f}_{i+\frac{1}{2}}^k = P_k\hat{f}_{i+\frac{1}{2}}^k. \quad (20)$$

According to the corollary, if the following equation

$$\tilde{f}_{i+\frac{1}{2}}^k = f_{i+\frac{1}{2}} - \frac{1}{24}\frac{\partial^2 f}{\partial x^2}\Big|_{i+\frac{1}{2}}\Delta x^2 + O(\Delta x^4), \quad (21)$$

is satisfied, then $\tilde{f}_{i+1/2}^k$ is a fourth-order flux. Substituting Eqs. (18), (19) and (21) into Eq. (20), there is

$$\begin{aligned}&\left(1 + b_k\Delta x^3 + O(\Delta x^4)\right)\left(f_{i+\frac{1}{2}} - \frac{1}{24}\frac{\partial^2 f}{\partial x^2}\Big|_{i+\frac{1}{2}}\Delta x^2 + A_k\frac{\partial^3 f}{\partial x^3}\Big|_{i+\frac{1}{2}}\Delta x^3 + O(\Delta x^4)\right)\\ &= \left(f_{i+\frac{1}{2}} - \frac{1}{24}\frac{\partial^2 f}{\partial x^2}\Big|_{i+\frac{1}{2}}\Delta x^2 + O(\Delta x^4)\right). \quad (22)\end{aligned}$$

So, it is theoretically possible (assuming $f_{i+1/2} \neq 0$) to find that

$$b_k = -A_k\frac{\partial^3 f}{\partial x^3}\Big|_{i+\frac{1}{2}}\Big/ f_{i+\frac{1}{2}}. \quad (23)$$

Considering $\hat{f}_{i+1/2}^k = f_{i+1/2} + O(\Delta x^2)$ (Eq. (18)), a high order approximation of b_k can be found as

$$\tilde{b}_k = -A_k\frac{\partial^3 f}{\partial x^3}\Big|_{i+\frac{1}{2}}\Big/ \hat{f}_{i+\frac{1}{2}}^k. \quad (24)$$

Clearly, there is

$$\tilde{b}_k = b_k + O(\Delta x^2). \quad (25)$$

Hence, we obtain the perturbed fourth-order candidate fluxes as

$$\tilde{f}_{i+\frac{1}{2}}^k = (1 + \tilde{b}_k\Delta x^3)\hat{f}_{i+\frac{1}{2}}^k = \hat{f}_{i+\frac{1}{2}}^k - A_k\frac{\partial^3 f}{\partial x^3}\Big|_{i+\frac{1}{2}}\Delta x^3. \quad (26)$$

On stencil $S_5 = \{x_{i-2}, x_{i-1}, \cdots, x_{i+2}\}$, $\frac{\partial^3 f}{\partial x^3}\Big|_{i+1/2}$ can be discretized as

$$\frac{\partial^3 f}{\partial x^3}\Big|_{i+\frac{1}{2}} = \frac{-f_{i-2} + 2f_{i-1} - 2f_{i+1} + f_{i+2}}{2\Delta x^3} + O(\Delta x). \quad (27)$$

Substituting Eq. (27) into Eq. (26), the explicit form of the perturbed fluxes can be written as

$$\tilde{f}_{i+\frac{1}{2}}^k = \hat{f}_{i+\frac{1}{2}}^k - A_k(-f_{i-2} + 2f_{i-1} - 2f_{i+1} + f_{i+2})/2. \quad (28)$$

3.2.2. The weighted form of the perturbed fluxes

Using the perturbed fluxes $\tilde{f}^k_{i+1/2}$ Eq. (28), the numerical flux of a new weighted scheme can be written as

$$\tilde{f}_{i+\frac{1}{2}} = \sum_{k=0}^{2}\omega_k\tilde{f}^k_{i+\frac{1}{2}} = \sum_{k=0}^{2}\omega_k\hat{f}^k_{i+\frac{1}{2}} + \frac{(3\omega_0-\omega_1+\omega_2)}{24} \times\Big(-f_{i-2}+2f_{i-1}-2f_{i+1}+f_{i+2}\Big), \tag{29}$$

where ω_0, ω_1, ω_2 are the same weights of the WENO-Z scheme in Eq. (16).

Next, we derive the necessary and sufficient conditions for fifth-order convergence of Eq. (29). Directly applying the expansion form of $\sum_{k=0}^{2}\omega_k\hat{f}^k_{i\pm\frac{1}{2}}$ (Eqs. (15)–(17) in Ref.[4]) given by Borges et al., we have

$$\begin{aligned}\tilde{f}_{i\pm\frac{1}{2}} &= \Big(h_{i\pm\frac{1}{2}} + B^{\pm}\Delta x^5 + O(\Delta x^6)\Big) + \sum_{k=0}^{2}(\omega_k^{\pm}-c_k)\\ &\quad\times\left(h_{i\pm\frac{1}{2}} + A_k\frac{\partial^3 f}{\partial x^3}\Big|_{i\pm1/2}\Delta x^3 + D_k\Delta x^4 + O(\Delta x^5)\right)\\ &\quad+\frac{(3\omega_0^{\pm}-\omega_1^{\pm}+\omega_2^{\pm})}{12}\left(\frac{\partial^3 f}{\partial x^3}\Big|_{i\pm\frac{1}{2}}\Delta x^3 + O(\Delta x^4)\right)\\ &= \Big(h_{i\pm\frac{1}{2}} + B^{\pm}\Delta x^5 + O(\Delta x^6)\Big) + \sum_{k=0}^{2}(\omega_k^{\pm}-c_k)\\ &\quad\times\Big(h_{i\pm\frac{1}{2}} + D_k\Delta x^4 + O(\Delta x^5)\Big)\\ &\quad+\frac{(3\omega_0^{\pm}-\omega_1^{\pm}+\omega_2^{\pm})}{12}O(\Delta x^4),\end{aligned} \tag{30}$$

where $B^+ = B^-$, $D_0 = \frac{347}{1152}\frac{\partial^4 f}{\partial x^4}\Big|_i$, $D_1 = D_2 = -\frac{37}{1152}\frac{\partial^4 f}{\partial x^4}\Big|_i$.

Subtraction of the numerical fluxes in Eq. (30) gives

$$\begin{aligned}\frac{\tilde{f}_{i+\frac{1}{2}}-\tilde{f}_{i-\frac{1}{2}}}{\Delta x} &= f_i' + O(\Delta x^5) + \frac{\sum_{k=0}^{2}(\omega_k^{+}-c_k)h_{i+\frac{1}{2}} - \sum_{k=0}^{2}(\omega_k^{-}-c_k)h_{i-\frac{1}{2}}}{\Delta x}\\ &\quad+\sum_{k=0}^{2}D_k(\omega_k^{+}-\omega_k^{-})O(\Delta x^3) + \sum_{k=0}^{2}(\omega_k^{+}-c_k)O(\Delta x^4)\\ &\quad-\sum_{k=0}^{2}(\omega_k^{-}-c_k)O(\Delta x^4)\\ &\quad+\frac{3(\omega_0^{+}-\omega_0^{-})-(\omega_1^{+}-\omega_1^{-})+(\omega_2^{+}-\omega_2^{-})}{12}O(\Delta x^3).\end{aligned} \tag{31}$$

From Eq. (31), we obtain the necessary and sufficient conditions for the fifth-order convergence of the fifth-order weighted scheme Eq. (29) as

$$\omega_k^{+}-\omega_k^{-} = O(\Delta x^2), \tag{32a}$$

$$\omega_k^{\pm}-c_k = O(\Delta x). \tag{32b}$$

Comparing current necessary and sufficient conditions Eq. (32) with those of Eq. (14) derived from the traditional WENO schemes, we can find that the current ones relax the requirements on the weights by one order.

Clearly, a sufficient condition for fifth-order convergence of the new weighted scheme Eq. (29) can be obtained as

$$\omega_k^{\pm} = c_k + O(\Delta x^2). \tag{33}$$

3.2.3. The flux of the new P-WENO scheme

The form of Eq. (29) is constructed by following the weighting process of the WENO scheme, however, since the term $F^{(3)} := \frac{\partial^3 f}{\partial x^3}\big|_{i+1/2}\Delta x^3 = (-f_{i-2}+2f_{i-1}-2f_{i+1}+f_{i+2})/2$ is used in all perturbed candidate fluxes, the scheme Eq. (29) loses the ENO property. Fortunately, the term $F^{(3)}$ is independent of the traditional flux $\hat{f}_{i+1/2}$, hence it is easy to make the scheme have the ENO property by limiting the influence of $F^{(3)}$ if a discontinuous solution is solved. This paper suggests using a tunable function φ to play this role. The final flux of the weighted scheme with ENO property (P-WENO) is

$$\tilde{f}_{i+\frac{1}{2}} = \sum_{k=0}^{2}\omega_k\hat{f}^k_{i+\frac{1}{2}} + \frac{\varphi(3\omega_0-\omega_1+\omega_2)}{24} \times(-f_{i-2}+2f_{i-1}-2f_{i+1}+f_{i+2}). \tag{34}$$

For the function φ, it is required that

1) if the stencil $S_5 = (x_{i-2}, x_{i-1}, \cdots, x_{i+2})$ is a discontinuous stencil, then φ is a small value;
2) if the stencil S_5 is smooth, then φ does not affect the accuracy convergence of Eq. (29).

According to Eq. (33), a sufficient condition, which satisfies condition 2), can be derived as

$$\varphi = 1 + O(\Delta x^2). \tag{35}$$

In this paper, the function

$$\varphi = 1 - \left(\frac{\tau_5}{IS_0+IS_2+\varepsilon}\right)^2, \tag{36}$$

is suggested, where τ_5 is the global smoothness indicator of the WENO-Z scheme; IS_0, IS_2 are the local smoothness indicators in Eq. (13), ε is a small positive number introduced to avoid the denominator becoming zero. It is easy to verify that the function φ satisfies the designing requirements 1) and 2).

It should be pointed out that, the scheme Eq. (34) is different to the hybrid schemes, the second term in the right hand side is an approximation of the third derivative of the function f at $i+1/2$, rather than a numerical flux for discretizing the first derivative in the traditional hybrid scheme, and it can be regarded as an anti-dissipation term. Hence, the new scheme actually provides a novel method to decrease the numerical dissipation of traditional WENO schemes.

3.3. The accuracy analysis of the P-WENO scheme

Taylor expansions of Eq. (13) at x_i give

$$IS_k = \begin{cases} f_i'^2\Delta x^2 + O(\Delta x^4), & f_i' \neq 0,\\ \frac{13}{12}f_i''^2\Delta x^4 + O(\Delta x^5), & f_i' = 0.\end{cases} \tag{37}$$

Then, we obtain

$$\tau_5 = \begin{cases} \left|\frac{13}{3}f_i''f_i''' - f_i'f_i^{(4)}\right|\Delta x^5 + O(\Delta x^7), & f_i' \neq 0,\\ \left|\frac{13}{3}f_i''f_i'''\right|\Delta x^5 + O(\Delta x^7), & f_i' = 0.\end{cases} \tag{38}$$

Similar to the analysis in [5], substituting Eqs. (37) and (38) into Eq. (16), there is

$$\alpha_k = \begin{cases} c_kE_{\Delta x}\big(1+O(\Delta x^5)\big), & f_i' \neq 0,\\ c_kF_{\Delta x}\big(1+O(\Delta x^2)\big), & f_i' = 0,\end{cases} \tag{39}$$

where

$$E_{\Delta x} = 1 + \left|\frac{13}{3}f_i''f_i''' - f_i'f_i^{(4)}\right| \Big/ f_i'^2\Delta x^3,$$
$$F_{\Delta x} = 1 + 4\left|f_i''f_i'''\right| \Big/ f_i'^2\Delta x. \tag{40}$$

Clearly, $E_{\Delta x}$ and $F_{\Delta x}$ are independent of k. Hence, we obtain

$$\omega_k = \begin{cases} c_k + O(\Delta x^5), & f_i' \neq 0,\\ c_k + O(\Delta x^2), & f_i' = 0.\end{cases} \tag{41}$$

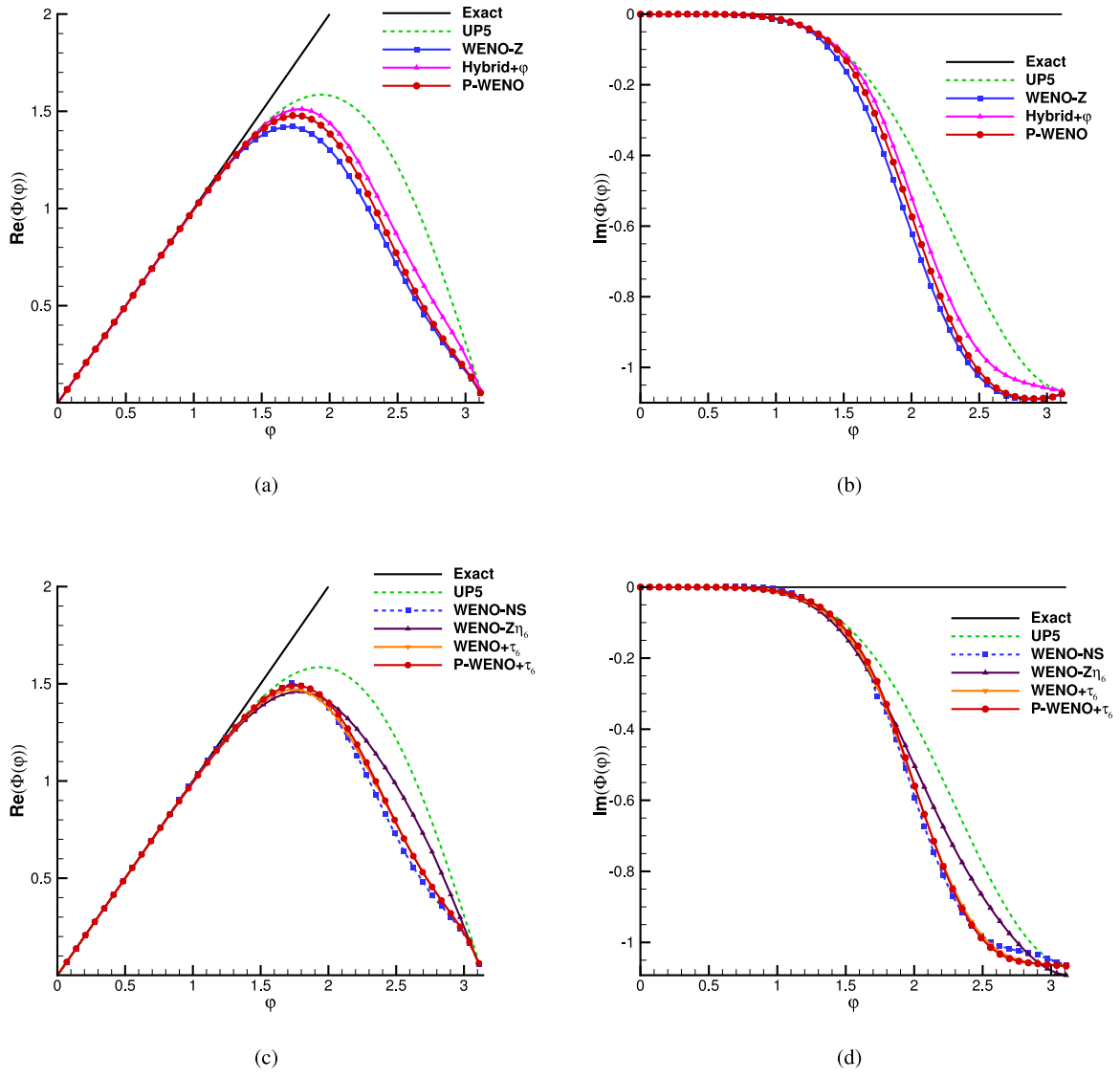

Fig. 1. Dispersion and dissipation properties for different schemes.

Eq. (41) indicates, the sufficient condition Eq. (33) for fifth-order convergence of the P-WENO scheme is satisfied. Hence, the P-WENO scheme is fifth-order accurate even at critical points.

It is worthy to point out that, there are several high order global smoothness indicators (GSI) proposed for improving the WENO-Z scheme, such as the sixth-order GSI ζ for WENO-NS [5], η_6 for WENO-Zη [7], τ_6 in Ref. [8]. Same as above analysis, using these high order GSIs, the calculated weights can meet the sufficient condition Eq. (15) at critical points, hence the corresponding WENO-Z type schemes are the fifth-order accurate schemes. Even so, the numerical results given in next section show that, the P-WENO scheme (Eqs. (34) and (36)) with the high order GSIs mentioned above can further reduce the numerical dissipation.

3.4. The spectral properties of the P-WENO scheme

The spectral properties of a difference scheme can be obtained by using the method proposed by Pirozzoli in [20]. For comparing, Fig. 1 gives these properties for the fifth-order upwind scheme (UP5), WENO-Z, P-WENO, Hybrid+φ, WENO-NS [5] ($\xi = 0.1$), WENO-Zη_6 [7], WENO+τ_6 and P-WENO+τ_6. Where, Hybrid+φ denotes the hybrid scheme with the flux of $\hat{f}_{i+1/2} = (1-\varphi)\hat{f}^{WENO-Z}_{i+1/2} + \varphi\hat{f}^{UP5}_{i+1/2}$, which is used to demonstrate the difference between the P-WENO and hybrid scheme. And WENO+τ_6 denotes the WENO-Z scheme with the weights calculated by using τ_6 to replace τ_5 in Eq. (16). τ_6 [8] is a sixth-order global smoothness indicator and given as

$$\tau_6 = (|f_0^{(1)}| - |f_2^{(1)}|)^2 + \frac{13}{12}(|f_0^{(2)}| - |f_2^{(2)}|)^2,$$
$$f_0^{(1)} = (f_{i-2} - 4f_{i-1} + 3f_i)/2, \quad f_2^{(1)} = (-3f_i + 4f_{i+1} - f_{i+2})/2,$$
$$f_0^{(2)} = (f_{i-2} - 2f_{i-1} + f_i), \qquad f_2^{(2)} = (f_i - 2f_{i+1} + f_{i+2}). \tag{42}$$

From Fig. 1(a) and (b) , we can see that the P-WENO scheme shows smaller dispersion and dissipation than the WENO-Z scheme. Although the hybrid scheme shows better spectral properties than P-WENO, but for the solutions with discontinuities (for example, see Fig. 2(a) and (b)), it is more dissipative than P-WENO. This fact demonstrates the anti-dissipation of P-WENO is effective for both smooth solution and discontinuous solution, while the hybrid scheme can only improve the accuracy of smooth solution. Fig. 1(c) and (d) show that, with the sixth-order global smoothness indicators, the P-WENO+τ_6 scheme can still reduce the dispersion and dissipation of the WENO+τ_6 scheme in the region of medium wavenumber, though the improvement is not so remark-

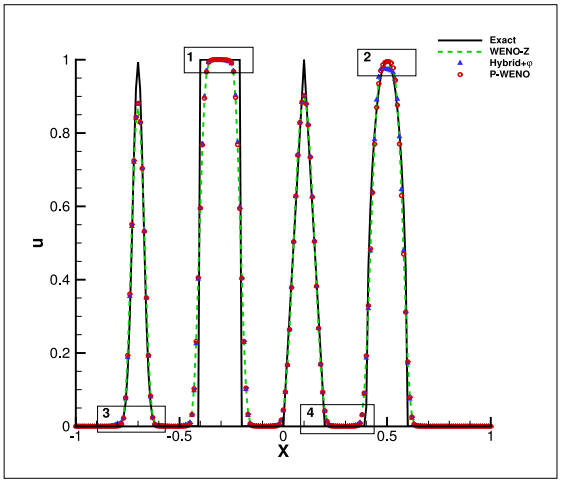

(a)

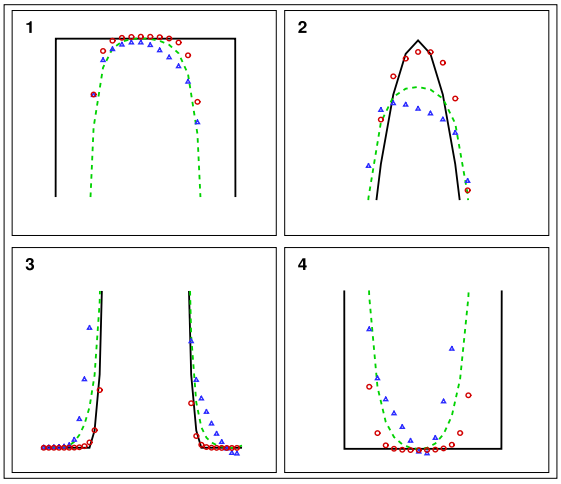

(b)

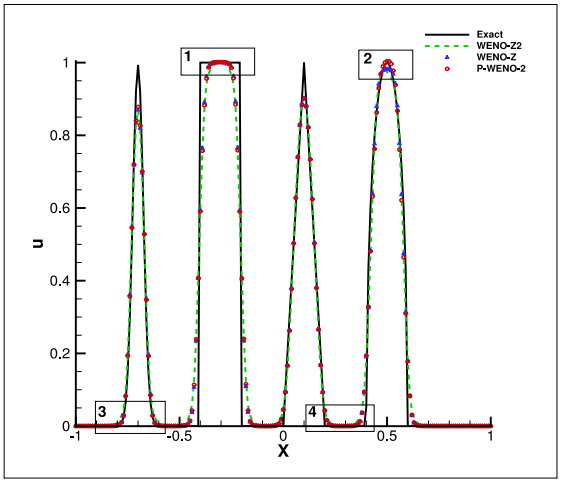

(c)

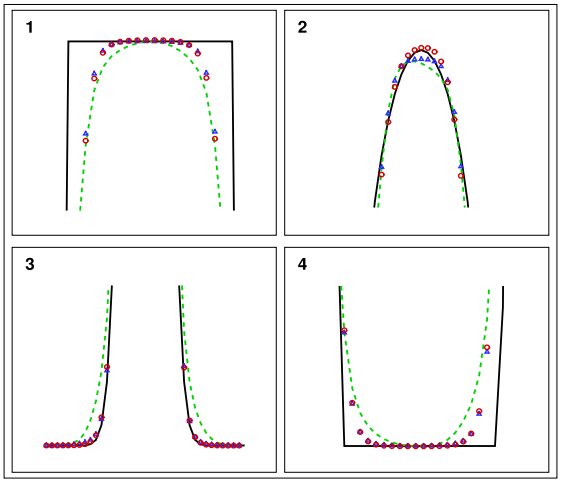

(d)

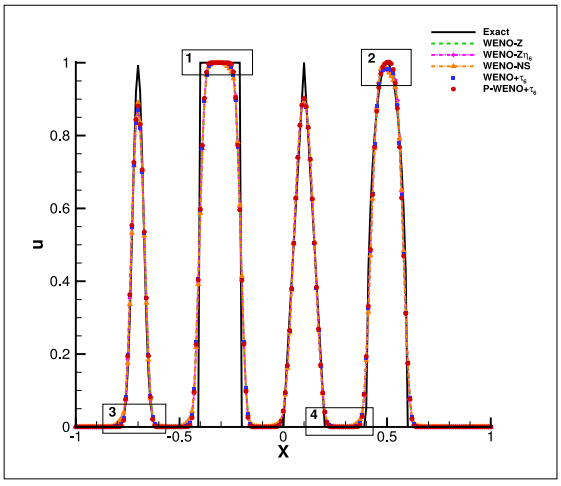

(e)

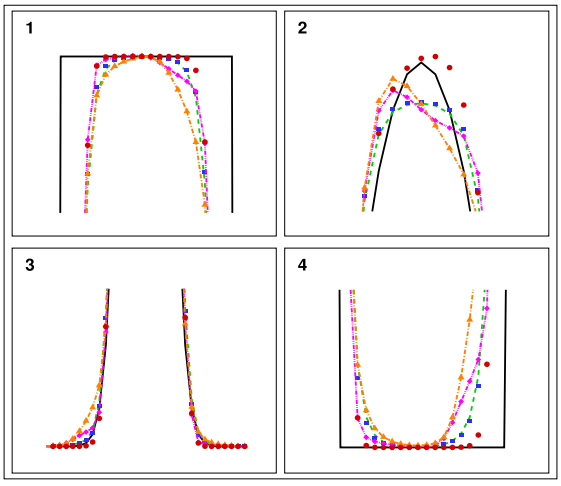

(f)

Fig. 2. Numerical results of the linear advection problem with initial condition Eq. (44) at $t = 6$, $N = 200$.

able as shown in the case with τ_5. In the region of high wavenumber, WENO-Zη_6 has less dispersion and dissipation than P-WENO, but it generates apparent asymmetry solution for the discontinuous problems (for example, the square wave and ellipse wave in Fig. 2(e) and (f)). In addition, these schemes, including Hybrid+φ, WENO-NS, WENO-Zη_6, may generate oscillation for the problems with strong shock waves (for example, the 1D problem of interacting blast waves in Section 4.3.2), and even cannot complete the computation.

Table 1
Comparison of errors and convergence orders for different schemes.

Δx	UP5		WENO-Z		P-WENO		Hybrid+φ	
	Error	order	Error	order	Error	order	Error	order
1/160	0.159E−12	–	0.870E−08	–	0.804E−10	–	0.133E−10	–
1/320	0.497E−14	5.00	0.770E−09	3.50	0.219E−11	5.20	0.738E−13	7.50
1/640	0.155E−15	5.00	0.559E−10	3.78	0.699E−13	4.97	0.366E−14	4.33
1/1280	0.485E−17	5.00	0.375E−11	3.90	0.227E−14	4.95	0.796E−16	5.52
Δx	WENO-NS		WENO-Zη_6		WENO+τ_6		P-WENO+τ_6	
1/160	0.145E−09	–	0.291E−10	–	0.311E−09	–	0.287E−11	–
1/320	0.570E−11	4.67	0.136E−11	4.42	0.145E−10	4.42	0.417E−13	6.10
1/640	0.194E−12	4.87	0.496E−13	4.78	0.527E−12	4.78	0.568E−15	6.20
1/1280	0.631E−14	4.94	0.166E−14	4.90	0.177E−13	4.90	0.641E−17	6.47

4. Numerical results

In this section, several numerical examples are presented to demonstrate the accuracy, robustness and resolution of the proposed perturbational WENO scheme. The fourth-order Runge-Kutta method [17] is used to approximate the time derivative, and the CFL number is set to be 0.5 for all examples in this paper, unless otherwise stated.

4.1. The accuracy at critical point

As used in Refs.[3,4], the function $f(x) = x^3 + \cos(x)$ is also used in this paper to measure the accuracy of the new scheme. $x = 0$ is a critical point where $f'(0) = 0$ and $f''(0) \neq 0$. Table 1 gives the errors and convergence orders of different schemes. We can see that, the original WENO-Z scheme is only fourth order, and the P-WENO scheme achieves fifth-order accuracy. It is worthy to point out that, for the smooth solution, the errors of the Hybrid+φ scheme is close to those of the fifth-order upwind scheme (UP5). However, for a solution containing complex structures, the hybrid scheme behaves even worse than the WENO-Z scheme, see the next case. It can also be seen that, with the sixth-order global smoothness indicators, the WENO-NS, WENO-Zη_6 and WENO+τ_6 schemes are fifth-order accurate, but the errors of P-WENO+τ_6 are at least one order of magnitude (some of them are even three orders) lower than the three schemes.

Compared with the hybrid scheme, the P-WENO+τ_6 scheme still reduces the errors with one order of magnitude in the cases with refined meshes. Another main advantage over the hybrid scheme is that the P-WENO scheme can effectively reduce the dissipation for the problems with shock waves, as analyzed in previous section and numerically shown in the next example.

4.2. One-dimensional linear advection problem

The governing equation of linear advection problem is given by

$$\begin{cases} \frac{\partial u}{\partial t} + \frac{\partial u}{\partial x} = 0, & x \in [-1, 1] \\ u(x, 0) = u_0(x), & \text{periodic boundary} \end{cases} \tag{43}$$

The initial condition of the first case, which contains a Gaussian, a square-wave, a triangle and a semi-ellipse wave, is given by

$$u(x,0) = \begin{cases} \frac{1}{6}(G(x,\beta,z-\delta) + G(x,\beta,z+\delta) + 4G(x,\beta,z)), & -0.8 \leqslant x \leq -0.6 \\ 1, & -0.4 \leqslant x \leq -0.2 \\ 1 - |10(x-0.1)|, & 0 \leqslant x \leq 0.2 \\ \frac{1}{6}(F(x,\alpha,a-\delta) + F(x,\alpha,a+\delta) + 4F(x,\alpha,a)), & 0.4 \leqslant x \leq 0.6 \\ 0, & \text{otherwise} \end{cases} \tag{44}$$

where $G(x,\beta,z) = e^{-\beta(x-z)^2}$, $F(x,\alpha,a) = \sqrt{max(1-\alpha^2(x-a)^2, 0)}$, $a = 0.5$, $z = -0.7$, $\delta = 0.005$, $\alpha = 10$ and $\beta = log2/36\delta^2$.

Fig. 2 gives the numerical results of different schemes with $N = 200$ at $t = 6$. Although the hybrid scheme behaves well for a smooth solution as shown in the previous case, it is even worse than the WENO-Z scheme in this case. This is possibly caused by frequent switches of different numerical fluxes. The P-WENO scheme behaves best for four kinds of waves. As shown in Fig. 2(c) and (d), for discontinuous problems, the WENO-Z2 (with the power $q = 2$) scheme increases the dissipation of the WENO-Z scheme, but the P-WENO-2 scheme (the P-WENO scheme with $q = 2$) shows similar dissipation as the WENO-Z ($q = 1$) scheme. Fig. 2(e) and (e) show that, the WENO-Zη_6 and WENO-NS ($\xi = 0.4$) schemes generate apparent asymmetry for the square wave and the semi-ellipse wave, while the P-WENO+τ_6 scheme not only improves the resolution near discontinuities over the others, but also keeps the wave shape well.

The initial condition of the second case is given by

$$u(x,0) = sin\left(\pi x - \frac{sin(\pi x)}{\pi}\right). \tag{45}$$

This solution has two critical points, where $f' = 0$ and $f''' \neq 0$. As in Refs. [2,5], the time step is set to $\Delta x^{5/4}$. The program with quadruple precision is performed on Intel Xeon E5-2640 v3. Table 2 gives the errors, convergence orders and CPU time of different schemes at $t = 2$. The L_∞ norm of the error is computed by

$$L_\infty = max|u_i - u_{exact,i}|, \quad \text{for} \quad i = 1, \cdots N. \tag{46}$$

It can be seen that the convergence orders of the WENO-Z scheme gradually decrease to fourth order with refined grids, while the other schemes have almost the same errors and fifth-order convergence orders. Fig. 3 shows the computational efficiency. It can be seen that, P-WENO and Hybrid+φ cost about 20% and 15% CPU time more than WENO-Z, respectively. However, if the high accuracy (for example, $L_\infty < 1 \times 10^{-9}$ for this case) is required, both two schemes are more efficient than the WENO-Z scheme. With the sixth-order global smoothness indicators (Fig. 3(b)), since all the four schemes (WENO-NS ($\xi = 0.1$), WENO-Zη_6, WENO+τ_6, P-WENO+τ_6) are of fifth-order, P-WENO+τ_6 cannot improve the efficiency for a simple smooth solution.

Table 2
Comparison of errors, convergence orders and CPU time (in seconds) for different schemes.

N	UP5		WENO-Z		P-WENO		Hybrid+φ	
	L_∞(order)	CPU time	L_∞(order)	CPU time	L_∞(order)	CPU time	L_∞(order)	CPU time
160	0.21E−06(−)	1.4E−01	0.21E−06(−)	7.2E−01	0.21E−06 (−)	8.6E−01	0.21E−06 (−)	8.2E−01
320	0.66E−08(5.00)	6.6E−01	0.78E−08(4.76)	3.3E+00	0.66E−08(5.00)	4.0E+00	0.66E−08(5.00)	3.8E+00
640	0.20E−09(5.00)	3.1E+00	0.36E−09(4.44)	1.6E+01	0.20E−09(5.00)	1.9E+01	0.20E−09(5.00)	1.8E+01
1280	0.64E−11(5.00)	1.5E+01	0.17E−10(4.37)	7.3E+01	0.64E−11(5.00)	8.9E+01	0.64E−11(5.00)	8.5E+01
2560	0.20E−12(5.00)	6.9E+01	0.82E−12(4.39)	3.4E+02	0.20E−12(5.00)	4.2E+02	0.20E−12(5.00)	4.0E+02
N	WENO-NS		WENO-Zη_6		WENO+τ_6		P-WENO+τ_6	
160	0.21E−06(−)	7.8E−01	0.21E−06(−)	9.2E−01	0.21E−06 (−)	8.1E−01	0.21E−06 (−)	9.6E−01
320	0.66E−08(5.00)	3.6E−00	0.66E−08(5.00)	4.2E+00	0.66E−08(5.00)	3.8E+00	0.66E−08(5.00)	4.5E+00
640	0.20E−09(5.00)	1.7E+01	0.20E−09(5.00)	2.0E+01	0.20E−09(5.00)	1.8E+01	0.20E−09(5.00)	2.1E+01
1280	0.64E−11(5.00)	7.9E+01	0.64E−11(5.00)	9.3E+01	0.64E−11(5.00)	8.4E+01	0.64E−11(5.00)	9.9E+01
2560	0.20E−12(5.00)	3.7E+02	0.20E−12(5.00)	4.4E+02	0.20E−12(5.00)	4.0E+02	0.20E−12(5.00)	4.7E+02

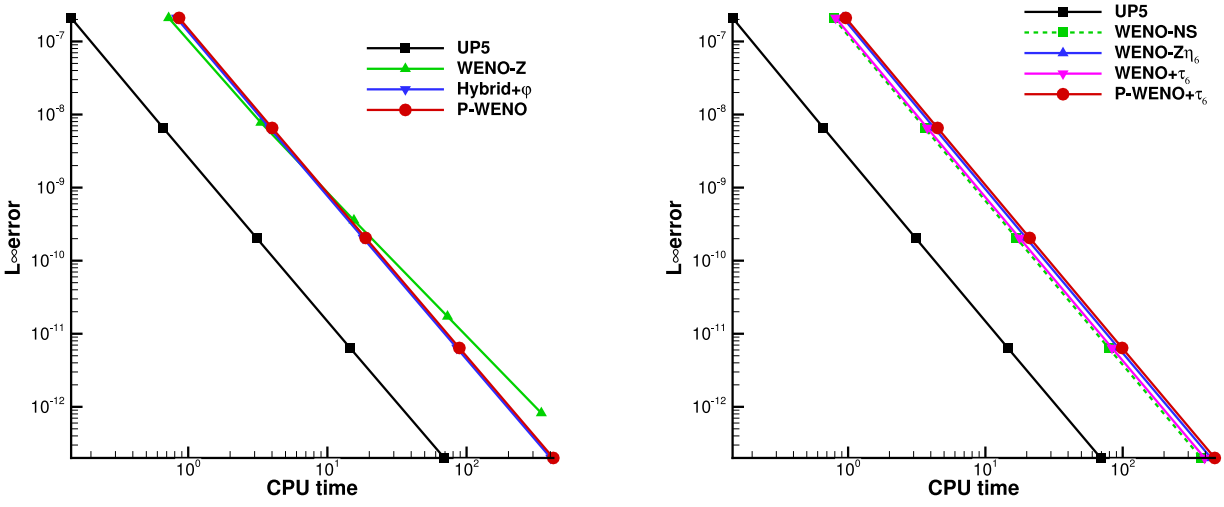

(a) (b)

Fig. 3. Comparisons of computational efficiency.

4.3. One-dimensional Euler problems

The governing equation of one-dimensional Euler problems is given by

$$\frac{\partial U}{\partial t}+\frac{\partial F(U)}{\partial x}=0, \tag{47}$$

where $U=(\rho,\rho u,E)^T, F(U)=\left(\rho u,\rho u^2+p,u(E+p)\right)^T$; ρ, u, E, p denote the density, velocity, total energy and pressure, respectively. For ideal gas, $E=\frac{p}{\gamma-1}+\frac{1}{2}\rho u^2$. $\gamma=1.4$ is the ratio of specific heat. The global LF flux-splitting method is used and the reconstruction is carried out in local characteristic fields.

4.3.1. Shock entropy wave interaction

The initial conditions of this problem are

$$(\rho,u,p)=\begin{cases}(3.857143,2.629369,31/3), & -5\le x<-4\\ (1+0.2sin(5x),0,1), & -4\le x\le 5\end{cases} \tag{48}$$

This problem describes the interaction of a Mach 3 shock wave with sine waves and is often used to evaluate the accuracy and numerical dissipation of a scheme. Fig. 4 gives the comparison of numerical results with $N=200$ at $t=1.8$. The reference solution is computed by the WENO-Z scheme with refined grids. As shown in Fig. 4(a), both the P-WENO and Hybrid+φ schemes are more accurate than the WENO-Z scheme. Similarly, with the sixth-order global smoothness indicators (Fig. 4(b)), the three schemes (WENO-Zη_6, WENO-NS ($\xi=0.4$) and P-WENO+τ_6) seem better than WENO+τ_6. However, further comparisons show that, if these schemes are applied to solve the problems with strong shock waves (for example, the next case of Section 4.3.2), the numerical dissipation of these schemes, such as Hybrid+φ, WENO-Zη_6, WENO-NS and P-WENO+τ_6, is not enough to suppress the spurious oscillation.

4.3.2. Interacting blast waves

The initial conditions of this problem are

$$(\rho,u,p)=\begin{cases}(1,0,1000), & 0\le x<0.1\\ (1,0,0.01), & 0.1\le x<0.9\\ (1,0,100), & 0.9\le x\le 1\end{cases} \tag{49}$$

The initial pressure gradients generate two interacting density shock waves. It is usually used to test the robustness and the capability of shock-capturing of schemes. For this case, only the three schemes (WENO-Z, P-WENO and WENO+τ_6) can obtain the results at $t=0.038$ (see Fig. 5), and the other schemes can not complete the computation. The reason is that their numerical dissipation is not enough to suppress the spurious oscillation. Fig. 5 shows that P-WENO and WENO+τ_6 obtain nearly overlapped solution, and they improve the solution of the WENO-Z scheme near extreme points.

The comprehensive comparisons, such as accuracy at critical point (Table 1 shows P-WENO is more accurate than WENO-Z

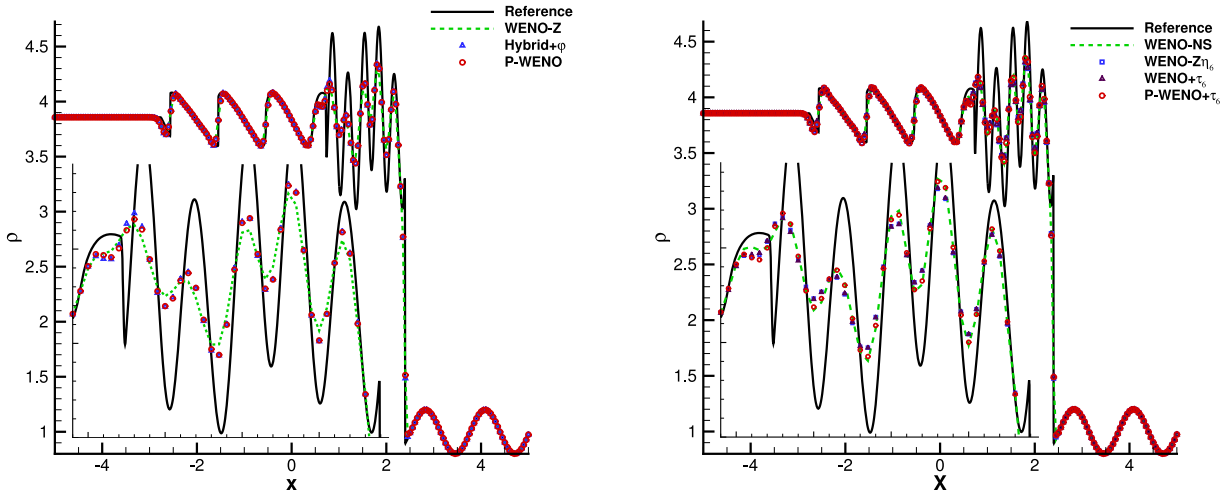

Fig. 4. Shock entropy wave interaction, $t = 1.8$, $N = 200$.

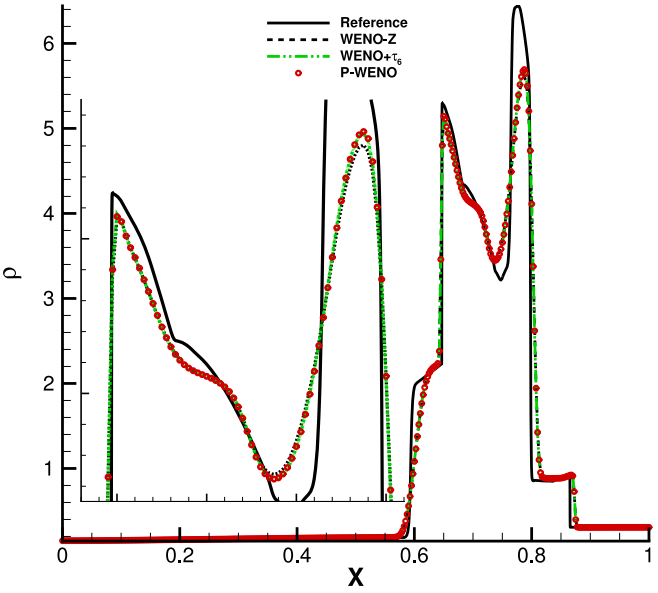

Fig. 5. Interacting blast waves, $t = 0.038$, $N = 400$.

and WENO+τ_6), the accuracy order (P-WENO and WENO+τ_6 obtain identical results, they are more accurate than WENO-Z, see Table 2), the resolution of complex wave structure (Fig. 2 shows P-WENO is better than WENO-Z and WENO+τ_6), and the almost same robustness for solving the problems with strong shock waves (the problem of interacting blast waves, i.e. Fig. 5. Except WENO-Z, WENO+τ_6 and P-WENO, the other schemes even cannot complete the computation), show that P-WENO is a beneficial scheme for simulating complex flows. Hence, in the rest of the examples in this paper, only the P-WENO and WENO-Z schemes are compared to demonstrate the advantages of the P-WENO scheme.

4.4. Two-dimensional Euler problems

The governing equation of two-dimensional Euler problems is given by

$$\frac{\partial U}{\partial t} + \frac{\partial F(U)}{\partial x} + \frac{\partial G(U)}{\partial y} = 0, \tag{50}$$

where

$$\begin{aligned} U &= (\rho, \rho u, \rho v, E)^T, \\ F(U) &= (\rho u, \rho u^2 + p, \rho uv, (E+p)u)^T, \\ G(U) &= (\rho v, \rho uv, \rho v^2 + p, (E+p)v)^T. \end{aligned} \tag{51}$$

The specific total energy E is given by

$$E = \frac{p}{(\gamma - 1)} + \frac{1}{2}\rho(u^2 + v^2). \tag{52}$$

The Steger–Warming [21] flux splitting method is used for the inviscid convective fluxes. The time step is taken as [22]

$$\Delta t = CFL\frac{\Delta t_x \Delta t_y}{\Delta t_x + \Delta t_y}, \quad \text{with } \Delta t_x = \frac{\Delta x}{\max_{i,j}(|u_{i,j}| + c_{i,j})} \text{ and}$$

$$\Delta t_y = \frac{\Delta y}{\max_{i,j}(|v_{i,j}| + c_{i,j})}, \tag{53}$$

where c is the speed of sound.

4.4.1. Two-dimensional vortex evolution problem

The two-dimensional vortex evolution problem is often used to evaluate the dissipation property of a scheme. It describes an isentropic vortex moves across the computational domain periodically. The initial conditions of this problem are

$$\begin{cases} u = 0.5 - \frac{\varepsilon e^{(1-r^2)/2}}{2\pi}(y-5), \\ v = \frac{\varepsilon e^{(1-r^2)/2}}{2\pi}(x-5), \\ T = 1 - \frac{(\gamma-1)\varepsilon^2 e^{(1-r^2)}}{8\gamma\pi^2}, \\ S = 1. \end{cases} \tag{54}$$

The temperature T and entropy S are defined as follows

$$T = \frac{p}{\rho}, \qquad S = \frac{p}{\rho^\gamma}.$$

where $r^2 = (x-5)^2 + (y-5)^2$, and vortex strength ε is 0.5. The computational domain is $[0, 10] \times [0, 10]$. Periodic boundary conditions are set for all boundaries. Figs. 6 and 7 give the pressure contours and integrated kinetic energy ($E_k = \sum_{i,j} \rho_{i,j}(u_{i,j}^2 + v_{i,j}^2)/2$) evolution with $N_x \times N_y = 50 \times 50$ at $t = 800$, respectively. It can be seen that, the P-WENO scheme is less dissipative than the WENO-Z scheme, its results are close to those of the fifth-order upstream scheme (UP5).

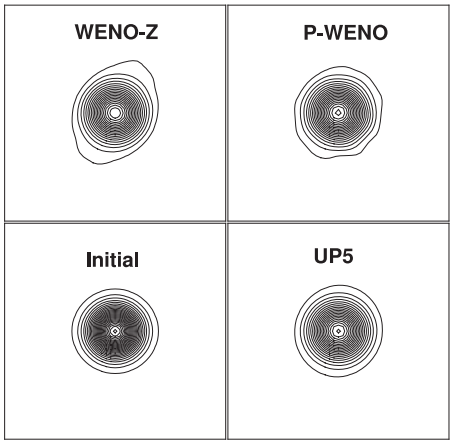

Fig. 6. Pressure contours of the vortex evolution problem, $t = 800$, 30 contours from 0.9905 to 0.9998.

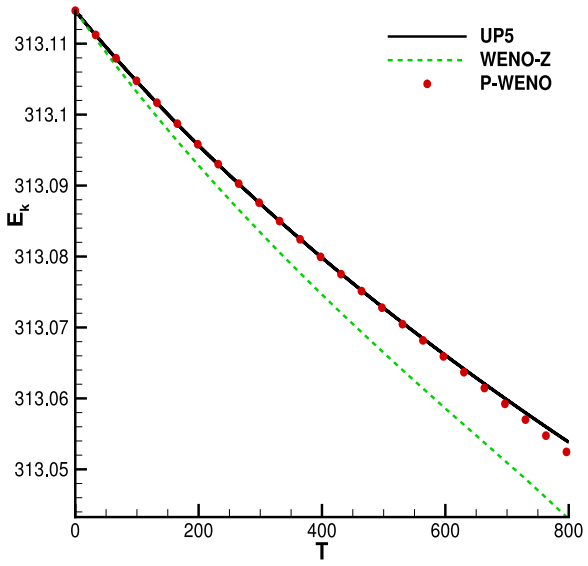

Fig. 7. Integrated kinetic energy versus time.

4.4.2. Rayleigh–Taylor instability

The initial conditions of this problem are

$$(\rho, u, v, p) = \begin{cases} (2, 0, -0.025\sqrt{\frac{5p}{3\rho}}\cos(8\pi x), 2y+1), & 0 \le y < 0.5 \\ (1, 0, -0.025\sqrt{\frac{5p}{3\rho}}\cos(8\pi x), y+\frac{3}{2}), & 0.5 \le y \le 1 \end{cases} \tag{55}$$

This problem describes the interface instability between fluids with different densities when an acceleration is directed from the heavy fluid to the light one, and it is often used to test the numerical dissipation of a high-order scheme [23,24]. The computational domain is $[0, 0.25] \times [0, 1]$. The top and bottom boundaries are set as $(\rho, u, v, p) = (1, 0, 0, 2.5)$ and $(\rho, u, v, p) = (2, 0, 0, 1)$, respectively. The reflective boundary conditions are set for the left and right boundaries. The gravitational effect is introduced by adding ρ and ρv to the right hand side of the y-momentum and the energy equations, respectively, i.e., the source term $S = (0, 0, \rho, \rho v)^T$ is added to the right-hand side of the Euler equations Eq. (50). The density contours with $N_x \times N_y = 240 \times 960$ at $t = 1.95$ is shown in Fig. 8. It can be seen that, both the WENO-Z and P-WENO schemes maintain symmetry of the flow structure well. Since the inviscid Euler equations are solved, the details of the complex instable structures are related to the numerical dissipation of the used scheme [25]. The richer instable structures obtained by the P-WENO scheme indicate that the P-WENO scheme is less dissipative than the original WENO-Z scheme.

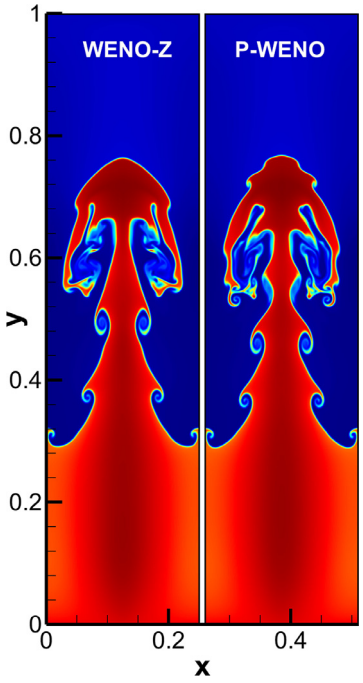

Fig. 8. Density contours of Rayleigh-Taylor instability, $N_x \times N_y = 240 \times 960$.

4.4.3. Two-dimensional Riemann problem

The initial conditions of this problem are

$$(\rho, u, v, p) = \begin{cases} (1.5, 0, 0, 1.5), & 0.8 \le x \le 1, 0.8 \le y \le 1 \\ (0.5323, 1.206, 0, 0.3), & 0 \le x < 0.8, 0.8 \le y \le 1 \\ (0.138, 1.206, 1.206, 0.029), & 0 \le x < 0.8, 0 \le y < 0.8 \\ (0.5323, 0, 1.206, 0.3), & 0.8 \le x \le 1, 0 \le y < 0.8 \end{cases} \tag{56}$$

This problem is proposed by Schulz-Rinne et al. [26] and usually used to test the capability for capturing different structures, such as reflection shocks, contact discontinuities and the instability interfaces. The computational domain is $[0, 1] \times [0, 1]$ and divided into four quadrants by two lines $x = 0.8$ and $y = 0.8$. Fig. 9 gives the density contours with $N_x \times N_y = 400 \times 400$ at $t = 0.8$. Both of the WENO-Z and P-WENO schemes obtain basically similar solution structures in the region where shocks interact with each other and can capture shocks well. Careful comparison of this figure, especially the region of $[1.35, 1.65] \times [0.35, 0.65]$, it can be found that the present scheme generates richer structures caused by Kelvin-Helmholtz instabilities than the WENO-Z scheme. The anti-dissipation term in the P-WENO scheme plays a key role.

4.5. Decaying isotropic turbulence [27]

The final case is that of decaying isotropic turbulence with eddy shocklets. The governing equation of this problem is the three-

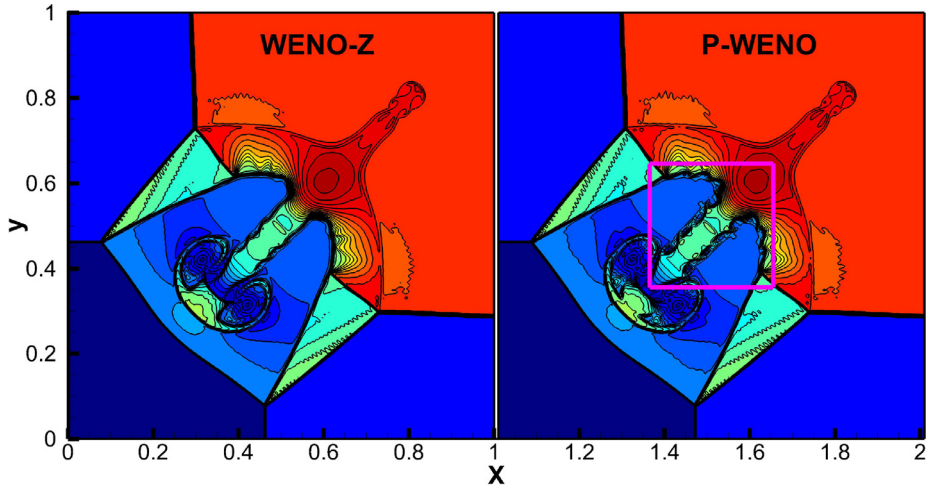

Fig. 9. Density contours of two-dimensional Riemann problem, $N_x \times N_y = 400 \times 400$, 30 contours from 0.2 to 1.85.

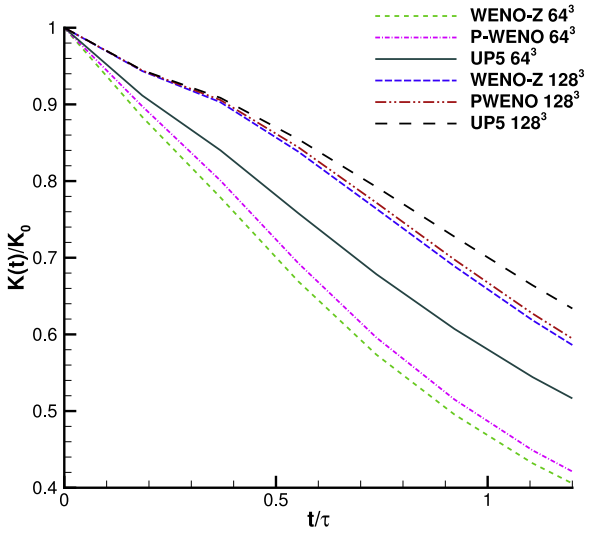

Fig. 10. Temporal evolution of normalized average kinetic energy.

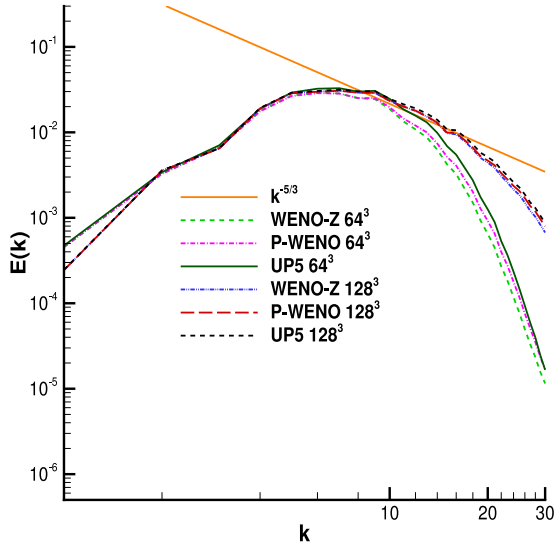

Fig. 11. Energy spectrum at $t/\tau = 1$ for decaying isotropic turbulence.

dimensional Navier-Stokes equations and is given by

$$\frac{\partial U}{\partial t} + \frac{\partial F}{\partial x} + \frac{\partial G}{\partial y} + \frac{\partial H}{\partial z} = \frac{1}{Re}\left(\frac{\partial F_v}{\partial x} + \frac{\partial G_v}{\partial y} + \frac{\partial H_v}{\partial z}\right), \tag{57}$$

where U is the conservative variables, F, G, H and F_v, G_v, H_v are the viscous and inviscid fluxes in $x-$, $y-$ and $z-$ directions, Re is Reynolds number. $\gamma = 1.4$ and $Pr = 0.7$. The computational domain is $[0, 2\pi]^3$ and periodic boundary conditions are set for all boundaries. The initial conditions of the thermodynamic quantity use the same conditions as those of the $IC4$ proposed by Samtaney et al. in [28], i.e., with constant pressure, density and temperature fields. And the initial velocity field satisfies a specified energy spectrum and given by

$$E(k) = Ak^4 exp(-2k^2/k_0^2), \tag{58}$$

where k is the wave number, k_0 is the wave number at which the spectrum peaks, and A is a constant chosen to get a specified initial kinetic energy. We set $A = 0.00013$ and $k_0 = 8$. The turbulent Mach number M_t and Taylor Reynolds number Re_λ, the definitions of which are defined in the Ref. [28], are set to be 0.3 and 72, respectively. The viscous terms are discretized with the sixth-order central difference scheme. The third-order TVD Runge-Kutta method [17] with the time step $\Delta t = 0.001$ is used for time advancing. Fig. 10 gives the temporal evolution of average kinetic energy $K(t)$ normalised by the initial kinetic energy $K_0 = \frac{3A}{64}\sqrt{2\pi}k_0^5$ with 64^3 and 128^3 grids for different schemes. Meanwhile, the energy spectrum at $t/\tau = 1$ ($\tau = \sqrt{\frac{32}{A}}(2\pi)^{\frac{1}{4}}k_0^{-\frac{7}{2}}$ is the initial large-eddy-turnover time) on the two grids is plotted in Fig. 11. The $k^{-5/3}$ law is used as a reference for the energy spectrum. As shown in these figures, the results of the P-WENO scheme is always located between the UP5 and WENO-Z schemes. Hence, P-WENO is less dissipative than WENO-Z for the simulation of decaying isotropic turbulence.

5. Conclusions

This paper proposes a perturbational weighted essentially non-oscillatory (P-WENO) scheme by weighting the perturbed candidate fluxes. The perturbed fluxes are one order higher than the ones used in the traditional fifth-order WENO schemes. The necessary and sufficient conditions for the fifth-order convergence of the P-WENO scheme are derived. They are one order lower than those derived by Henrick et al. for the traditional fifth-order WENO scheme. Theoretical analysis and numerical results show that the

P-WENO scheme can recover fifth-order at the critical points by using the same weights as used in the WENO-Z scheme. The second term in the P-WENO scheme plays the role of anti-dissipation, hence, using the same weights, whether they satisfy the sufficient condition of fifth-order convergence or not, the P-WENO-type schemes are less dissipative than the counterparts with traditional candidate fluxes. Various examples demonstrate that the P-WENO scheme is robust and low dissipative.

This paper presents a different method to develop high-order low-dissipation WENO schemes. The method can be easily extended to develop third order and higher-order (higher than fifth-order) perturbational WENO schemes.

Acknowledgement

This research work was supported by NSAF No. U1530145, NKRDPC No. 2016YFA0401200, SCP No. TZ2016002, and NSFC Nos. 11272325, 11272324.

Appendix. Proof of Corollary

Taylor expansions of $\frac{\partial^{2l} f}{\partial x^{2l}}\Big|_{i+1/2}$ and $\frac{\partial^{2l} f}{\partial x^{2l}}\Big|_{i-1/2}$ at x_i can be written as

$$\frac{\partial^{2l} f}{\partial x^{2l}}\Big|_{i+\frac{1}{2}} = \sum_{k=0}^{2(m-l+1)} \frac{1}{k!}\left(\frac{\Delta x}{2}\right)^k \frac{\partial^{2l+k} f}{\partial x^{2l+k}}\Big|_i + O(\Delta x^{k+1}),$$
$$\frac{\partial^{2l} f}{\partial x^{2l}}\Big|_{i-\frac{1}{2}} = \sum_{k=0}^{2(m-l+1)} \frac{1}{k!}\left(-\frac{\Delta x}{2}\right)^k \frac{\partial^{2l+k} f}{\partial x^{2l+k}}\Big|_i + O(\Delta x^{k+1}). \quad (59)$$

(1) $\tilde{A} \neq 0$

Substituting Eq. (59) into Eq. (7), we have

$$\begin{aligned}\hat{f}_{i+\frac{1}{2}} - \hat{f}_{i-\frac{1}{2}} &= \sum_{l=0}^{m} a_{2l}\Delta x^{2l}\left[\frac{\partial^{2l} f}{\partial x^{2l}}\Big|_{i+\frac{1}{2}} - \frac{\partial^{2l} f}{\partial x^{2l}}\Big|_{i-\frac{1}{2}}\right] \\ &\quad + \left(\tilde{A}\frac{\partial^{2m+1} f}{\partial x^{2m+1}}\Big|_{i+\frac{1}{2}} - \tilde{A}\frac{\partial^{2m+1} f}{\partial x^{2m+1}}\Big|_{i-\frac{1}{2}}\right)\Delta x^{2m+1} \\ &\quad + O(\Delta x^{2m+2}) \\ &= \sum_{l=0}^{m}\sum_{s=0}^{m-l} a_{2l}\frac{\Delta x^{2s+2l+1}}{2^{2s}(2s+1)!}\frac{\partial^{2s+2l+1} f}{\partial x^{2s+2l+1}}\Big|_i \\ &\quad + O(\Delta x^{2m+2}) + O(\Delta x^{2m+3}) \\ &= \sum_{l=0}^{m}\sum_{k=l}^{m} a_{2l}\frac{\Delta x^{2k+1}}{2^{2k-2l}(2k-2l+1)!}\frac{\partial^{2k+1} f}{\partial x^{2k+1}}\Big|_i \\ &\quad + O(\Delta x^{2m+2}) \\ &= \sum_{k=0}^{m}\sum_{l=0}^{k} a_{2l}\frac{\Delta x^{2k+1}}{2^{2k-2l}(2k-2l+1)!}\frac{\partial^{2k+1} f}{\partial x^{2k+1}}\Big|_i \\ &\quad + O(\Delta x^{2m+2}). \end{aligned} \quad (60)$$

If the coefficients a_{2l} satisfy Eq. (8), then the last formula of the right hand side of Eq. (60) is $a_0\frac{\partial f}{\partial x}\Big|_i \Delta x + O(\Delta x^{2m+2})$, thus

$$\frac{\hat{f}_{i+\frac{1}{2}} - \hat{f}_{i-\frac{1}{2}}}{\Delta x} = \frac{\partial f}{\partial x}\Big|_i + O(\Delta x^{2m+1}). \quad (61)$$

Therefore, the scheme is $(2m+1)$th order accurate.

(2) $\tilde{A} = 0$

Let

$$\hat{f}_{i\pm\frac{1}{2}} = \sum_{l=0}^{m} a_{2l}\Delta x^{2l}\frac{\partial^{2l} f}{\partial x^{2l}}\Big|_{i\pm\frac{1}{2}} + \tilde{B}\frac{\partial^{2m+2} f}{\partial x^{2m+2}}\Big|_{i\pm\frac{1}{2}}\Delta x^{2m+2} + O(\Delta x^{2m+3}), \quad (62)$$

where $\tilde{B}$ is a non-zero constant.

Substituting Eq. (59) into Eq. (62), we have

$$\begin{aligned}\hat{f}_{i+\frac{1}{2}} - \hat{f}_{i-\frac{1}{2}} &= \sum_{l=0}^{m} a_{2l}\Delta x^{2l}\left[\frac{\partial^{2l} f}{\partial x^{2l}}\Big|_{i+\frac{1}{2}} - \frac{\partial^{2l} f}{\partial x^{2l}}\Big|_{i-\frac{1}{2}}\right] \\ &\quad + \left(\tilde{B}\frac{\partial^{2m+2} f}{\partial x^{2m+2}}\Big|_{i+\frac{1}{2}} - \tilde{B}\frac{\partial^{2m+2} f}{\partial x^{2m+2}}\Big|_{i-\frac{1}{2}}\right)\Delta x^{2m+2} \\ &\quad + O(\Delta x^{2m+3}) \\ &= \sum_{l=0}^{m}\sum_{s=0}^{m-l} a_{2l}\frac{\Delta x^{2s+2l+1}}{2^{2s}(2s+1)!}\frac{\partial^{2s+2l+1} f}{\partial x^{2s+2l+1}}\Big|_i \\ &\quad + O(\Delta x^{2m+3}) \\ &= \sum_{l=0}^{m}\sum_{k=l}^{m} a_{2l}\frac{\Delta x^{2k+1}}{2^{2k-2l}(2k-2l+1)!}\frac{\partial^{2k+1} f}{\partial x^{2k+1}}\Big|_i \\ &\quad + O(\Delta x^{2m+3}) \\ &= \sum_{k=0}^{m}\sum_{l=0}^{k} a_{2l}\frac{\Delta x^{2k+1}}{2^{2k-2l}(2k-2l+1)!}\frac{\partial^{2k+1} f}{\partial x^{2k+1}}\Big|_i \\ &\quad + O(\Delta x^{2m+3}). \end{aligned} \quad (63)$$

If the coefficients a_{2l} satisfy the Eq. (8), then the last formula of the right hand side of Eq. (63) is $a_0\frac{\partial f}{\partial x}\Big|_i \Delta x + O(\Delta x^{2m+3})$, thus

$$\frac{\hat{f}_{i+\frac{1}{2}} - \hat{f}_{i-\frac{1}{2}}}{\Delta x} = \frac{\partial f}{\partial x}\Big|_i + O(\Delta x^{2m+2}). \quad (64)$$

Therefore, the scheme is $(2m+2)$th order accurate.

References

[1] Liu XD, Osher S, Chan T. Weighted essentially non-oscillatory schemes. J Comput Phys 1994;115:200–12.
[2] Jiang GS, Shu CW. Efficient implementation of weighted ENO schemes. J Comput Phys 1996;126:202–28.
[3] Henrick AK, Aslam TD, Powers JM. Mapped weighted essentially non-oscillatory schemes: achieving optimal order near critical points. J Comput Phys 2005;207:542–67.
[4] Borges R, Carmona M, Costa B, Don WS. An improved weighted essentially non-oscillatory scheme for hyperbolic conservation laws. J Comput Phys 2008;227:3191–211.
[5] Ha Y, Kim CH, Lee YJ, Yoon J. An improved weighted essentially non-oscillatory scheme with a new smoothness indicator. J Comput Phys 2013;232:68–86.
[6] Zhao S, Lardjane N, Fedioun I. Comparison of improved finite-difference WENO schemes for the implicit large eddy simulation of turbulent non-reacting and reacting high-speed shear flow. Comput Fluids 2014;95:74–87.
[7] Fan P, Shen YQ, Tian BL, Yang C. A new smoothness indicator for improving the weighted essentially non-oscillatory scheme. J Comput Phys 2014;269:329–54.
[8] Liu SP, Shen YQ, Zeng FJ, Yu M. A new weighting method for improving the WENO−Z scheme. Int J Numer Methods Fluids 2018;87:271–91.
[9] Castro M, Costa B, Don WS. High order weighted essentially non-oscillatory WENO-Z schemes for hyperbolic conservation laws. J Comput Phys 2011;230:1766–92.
[10] Arandiga F, Baeza A, Belda AM, Mulet P. Analysis of WENO schemes for full and global accuracy. SIAM J Numer Anal 2011;49:893–915.
[11] Don WS, Borges R. Accuracy of the weighted essentially non-oscillatory conservative finite difference schemes. J Comput Phys 2013;250:347–72.
[12] Gao Z, dynamics f. An infinite-order accurate upwind compact difference scheme for the convective diffusion equation. In: Proc of Asia workshop on computational, Sichuan, China; 1994. p. 50–6.
[13] Shen YQ, Gao Z, Yang DH. Second-order perturbational finite difference schemes for hyperbolic conservation equation. Acta Aerodyn Sin 2003;21:342–50.
[14] Gao Z, Yang GW. Perturbation finite volume method for the convection-diffusion integral equation. Acta Mech Sinica 2004;20:580–90.
[15] Li MJ, Yang YY, Shu S. Third-order modified coefficient scheme based on essentially non-oscillatory scheme. Appl Math Mech-Engl 2008;29:1477–86.
[16] Yu CH, Gao Z, TWH S. Development of a symplectic and phase error reducing perturbation finite-difference advection scheme. Numer Heat Transfer Part B 2016;70:136–51.
[17] Shu CW, Osher S. Efficient implementation of essentially non-oscillatory shock-capturing schemes. J Comput Phys 1988;77:439–71.
[18] Shui HS. The finite difference method of one-dimensional fluid dynamics. National Defense Industry Press; 1998.

[19] Shu CW, Osher S. Efficient implementation of essentially non-oscillatory shock capturing schemes II. J Comput Phys 1989;83:32–78.
[20] Pirozzoli S. On the spectral properties of shock-capturing scheme. J Comput Phys 2006;219:489–97.
[21] Steger SL, Warming RF. Flux vector splitting of the inviscid gasdynamic equations with application to finite-difference methods. J Comput Phys 1981;40:263–93.
[22] Pirozzoli S. Conservative hybrid compact-WENO schemes for shock-turbulence interaction. J Comput Phys 2002;178. 81–117
[23] Shi J, Zhang YT, Shu CW. Resolution of high order WENO schemes for complicated flow structures. J Comput Phys 2003;186:690–6.
[24] Arshed GM, Hoffmann KA. Minimizing errors from linear and nonlinear weights of WENO scheme for broadband applications with shock waves. J Comput Phys 2013;246:58–77.
[25] Xu ZF, Shu CW. Anti-diffusive flux corrections for high order finite difference WENO schemes. J Comput Phys 2005;205:458–85.
[26] Schulz-Rinne CW, Collins JP, Glaz HM. Numerical solution of the riemann problem for two-dimensional gas dynamics. J Sci Comput 1993;14:1394–414.
[27] Li XL, Fu DX, Ma YW. Direct numerical simulation of compressible isotropic turbulence. Sci China Ser A 2002;45:1452–60.
[28] Samtaney R, Pullin DI, Kosovic B. Direct numerical simulation of decaying compressible turbulence and shocklet statistics. Phys Fluids 2001;13:1415–30.